Global Variations in the Geoid/Topography Admittance of Venus

Mark Simons, Bradford H. Hager, Sean C. Solomon

Global representations of geoid height and topography are used to map variations in the geoid/topography ratio (admittance) of Venus. The admittance values are permissive of two mutually exclusive models for convection-driven topography. In the first, compressive highland plateaus are expressions of present mantle downwelling, broad volcanic rises are expressions of mantle upwelling, and lowlands overlie regions with no substantial vertical motion in the mantle. In the second, compressive highland plateaus are remnants of an earlier regime of high crustal strain, and most other long-wavelength topographic variations arise from normal convective tractions at the base of the lithosphere.

Convection is the primary means of heat loss for the silicate mantles of both Earth and Venus. Plate tectonics, the process by which oceanic lithosphere is formed at mid-ocean ridges and consumed at subduction zones, is a surface expression of mantle convection on Earth. Although Venus and Earth are similar in size, density, and bulk composition (*1*), radar images of the surface of Venus obtained by the recent Magellan mission show no evidence for global plate tectonics (*2, 3*). Thus, the surface manifestations of mantle convection are quite different on the two planets, a result plausibly attributed to the extreme dryness and high temperatures of the Venus surface (*1, 4, 5*). The high surface temperature makes the lithosphere on Venus more buoyant than its terrestrial counterpart and may inhibit the subduction process (*5*). Further, subduction requires throughgoing faulting of the entire thickness of the lithosphere, and most models of spatially localized brittle faulting require the presence of water (*6*). In the absence of water, the lithosphere of Venus may not be capable of faulting on the scale necessary to create plate boundaries (*7*).

The topography and gravity fields (*8*) measured by the Magellan spacecraft and the relation between them constitute crucial data, which we have used to develop models of the tectonic processes active on Venus. Variations in long-wavelength (greater than 700 km) geoid height (*9*) and surface topography are primary expressions of the underlying structure, mechanical constitution, and dynamics of the mantle-lithosphere system (*10*). The processes associated with mantle convection, lithospheric deformation, and the development of crustal thickness variations are not mutually exclusive, and their expressions are frequently interrelated. We can constrain how each of these processes influences a given region and horizontal scale by considering how variations in geoid height relate to variations in topography.

M. Simons and B. H. Hager are with the Department of Earth, Atmospheric, and Planetary Sciences, Massachusetts Institute of Technology, Cambridge, MA 02139, USA. S. C. Solomon is with the Department of Terrestrial Magnetism, Carnegie Institution of Washington, Washington, DC 20015, USA.

Geoid and topography are typically related through an admittance function, estimates of which have been used on Earth to calculate effective elastic plate thicknesses, crustal thicknesses, and dynamic stresses imparted by the convecting mantle (*11–13*). In its simplest usage, the admittance for a given area is the variation in geoid height divided by the variation in topography. Its sign and amplitude vary as a function of position and wavelength. At long wavelengths the geoid is most sensitive to processes associated with mantle convection. In the absence of significant long-wavelength topography associated with crustal thickness variations, a small or negative admittance value over a given area implies that a low-viscosity channel is present beneath the lithosphere, decoupling it from underlying stresses in the convecting mantle (*14*). Such a situation holds in oceanic regions on Earth (*13*). If crustal thickness variations are important, then the admittance can be used to determine the mean crustal thickness over a region. In the absence of mantle convective processes, the admittance for such areas is positive and increases as the crustal thickness increases.

Before the Magellan mission, tracking data from the Pioneer Venus Orbiter (PVO) indicated that the geoid height and topography of Venus are highly correlated on a planetary scale, but global analyses carried out with these data were limited to spherical harmonic degree and order 18 and less (wavelengths greater than ~2000 km), and only global averages of the admittance were obtained (*15, 16*). Several studies made use of line-of-sight (LOS) accelerations (*8*) of the PVO spacecraft over limited geographic areas on Venus to demonstrate that geoid height and topography correlate on shorter scales (~600 to ~2000 km) than could be represented with the global spherical harmonic fields then available, but such studies were limited to selected highland regions (*17–20*).

We present maps of geoid/topography admittances for most of Venus from data recently obtained during the Magellan mission (*21*). These maps demonstrate global variations in the admittance and constitute a guide to the depths and modes of compensation of topography associated with different large-scale features over much of Venus. We restrict our attention to the area north of 60°S (*22*), which occupies 93% of the surface of Venus and includes a wide range of geological structures (Fig. 1). The equatorial highlands of Aphrodite Terra span half the circumference of the planet. Western Aphrodite Terra consists of Ovda and Thetis Regiones, steep-flanked highlands rising ~3 km above the planetary mean and characterized by pervasive, dominantly compressive deformational features (*2*). In contrast, eastern Aphrodite Terra encompasses a broad rise, Atla Regio, topped by rift valleys and large volcanoes, with little evidence for compressional deformation (*2, 23*). Beta and Eistla Regiones are each similarly characterized by a topographic rise, large volcanoes, and rifting (*2, 23*). Alpha and Tellus Regiones are areas of tesserae, complexly deformed terrain much like western Aphrodite (*2, 24*). Ishtar Terra, which encompasses several mountain belts and blocks of highly deformed terrain (*2, 25, 26*), is the second largest compressionally deformed highland. Plains and lowlands, the lowest of which is Atalanta Planitia, lie between the highland terrains and make up most of the Venus surface. Ridge belts, compressional features with hundreds of meters of relief and dimensions of up to several thousand kilometers in length and hundreds of kilometers in width, are frequently associated with lowlands (*2, 27*).

Previous investigations of geoid-topography relations on Venus made use of geoid-to-topography ratios (GTR), estimates of the covariation of geoid height and surface elevation expressed as a function of position. The use of a single GTR relies on the premise that topography is locally compensated at one depth (28). The admittance is the equivalent to GTR in the wave number domain (29), but the assumption of a single compensation depth is not required because the admittance can vary with wavelength.

Following the practice in terrestrial studies, we assume that geoid and topography are linearly related and determine the admittance in a least squares sense (11, 28, 30). We cast the problem directly in terms of the global spherical harmonic coefficients, with geoid height N and topography H defined at colatitude θ and longitude ϕ by

$$N(\theta,\phi) = \mathrm{Re}\left[C_N \sum_{l=l_{\min}}^{l_{\max}} \sum_{m=-l}^{l} G_{lm} Y_{lm}(\theta,\phi)\right] \quad (1)$$

$$H(\theta,\phi) = \mathrm{Re}\left[C_H \sum_{l=l_{\min}}^{l_{\max}} \sum_{m=-l}^{l} T_{lm} Y_{lm}(\theta,\phi)\right] \quad (2)$$

where C_N and C_H are constants, G_{lm} and T_{lm} are spherical harmonic coefficients, Y_{lm} is the fully normalized complex spherical harmonic basis function of degree l and order m, and Re denotes the real part of the enclosed expression. We assume a relation of the form

$$G_{lm} = F_l T_{lm} + I_{lm} \quad (3)$$

where I_{lm} is the part of the geoid not linearly related to topography (30). The global admittance, F_l, for a single harmonic degree l, is defined as

$$F_l = \mathrm{Re}\left[\frac{\sigma_{gt}^2}{\sigma_{tt}^2}\right] \quad (4)$$

where σ_{gt} is the cross-covariance of geoid and topography, and σ_{tt} is the covariance of topography (30).

We define the cross-covariance function so as to determine regional variations, rather than only a global average, of the admittance. Calculations are simplified if we restrict ourselves to a regional domain, Ω, in the shape of a spherical cap, and if we adopt a reference frame whose pole pierces the center of this cap. In this reference frame, we define the covariance function, σ_{ab}, between global fields A and B as

$$\sigma_{ab}^2 = \left(\frac{1}{n}\right) \sum_{l_1=l_{\min}}^{l_{\max}} \sum_{l_2=l_{\min}}^{l_{\max}} \sum_{m=-m_0}^{m_0} A_{l_1m} B^*_{l_2m} W_{l_1l_2m} \quad (5)$$

where

$$W_{l_1l_2m} = \iint_{\Omega} Y_{l_1m} Y^*_{l_2m} d\Omega \quad (6)$$

$$n = \sum_{l_1=l_{\min}}^{l_{\max}} \sum_{l_2=l_{\min}}^{l_{\max}} \sum_{m=-m_0}^{m_0} W_{l_1l_2m} \quad (7)$$

$$m_0 = \min(l_1, l_2) \quad (8)$$

and an asterisk denotes complex conjugate. The admittance calculated from Eqs. 4 and 5 is an average, $\overline{F}$, over a band of harmonic degrees (31). Implicit in this formulation is the premise that the admittance can be represented by a single value over a given band but may vary among bands.

This procedure is repeated over a grid to create a map of admittance values. For each location, the spherical harmonic coefficients G_{lm} and T_{lm} are recalculated in the rotated reference frame. To reduce edge effects, we chose the diameter of the cap D_w to be 10% greater than the longest wavelength included in the analysis. Because $\overline{F}$ is the admittance over the whole cap, it is important when analyzing the maps to bear in mind the smoothing effect of finite cap diameter. We calculated results for six partially overlapping wave number bands spanning the range l = 10 to 55. We also made global maps for two of these bands: l = 10 to 14 with D_w = 4000 km (band 1) and l = 15 to 30 with D_w = 2700 km (band 3).

To compare our results to those of previous analyses, we applied our technique first to Earth (32). Admittance values range from −6 to 12 m/km for band 1 and −4 to 12 m/km for band 3. The continents are characterized by positive admittances of 4 to 8 m/km, consistent with Airy compensation of topography and average crustal thicknesses of about 50 km. The lowest admittances occur in oceanic regions near triple junctions and subduction zones. For example, the admittance over the Aleutian trench in band 1 is −4 ± 3 m/km (Fig. 2A). Given the strong sensitivity of the sign and amplitude of the admittance to mantle viscosity structure (33), one hypothesis (not tested here) is that these low admittances reflect horizontal variations in the effective viscosity of the upper mantle. In contrast, the admittance is higher near intraplate hot spots. For example, the admittance for the Hawaiian hot spot is about 10 m/km in band 1 and 6 m/km in band 3 (Fig. 2B). These values correspond to an apparent depth of compensation (ADC) of about 70 km for the Hawaiian hot spot, which agrees with previous estimates for the compensation depth of the swell (13).

Global (Fig. 2C) and regional (Fig. 2, D through L, and Fig. 3) admittance values for Venus (34, 35) range from 1 to 40 m/km (36), several times greater than the range for Earth in a given band. The globally averaged admittance is not well matched by an Airy model. The steady increase in admittance with decreasing wave number, however, is similar to predictions from models of mantle convection with no crustal thickness variations (37, 38). Admit-

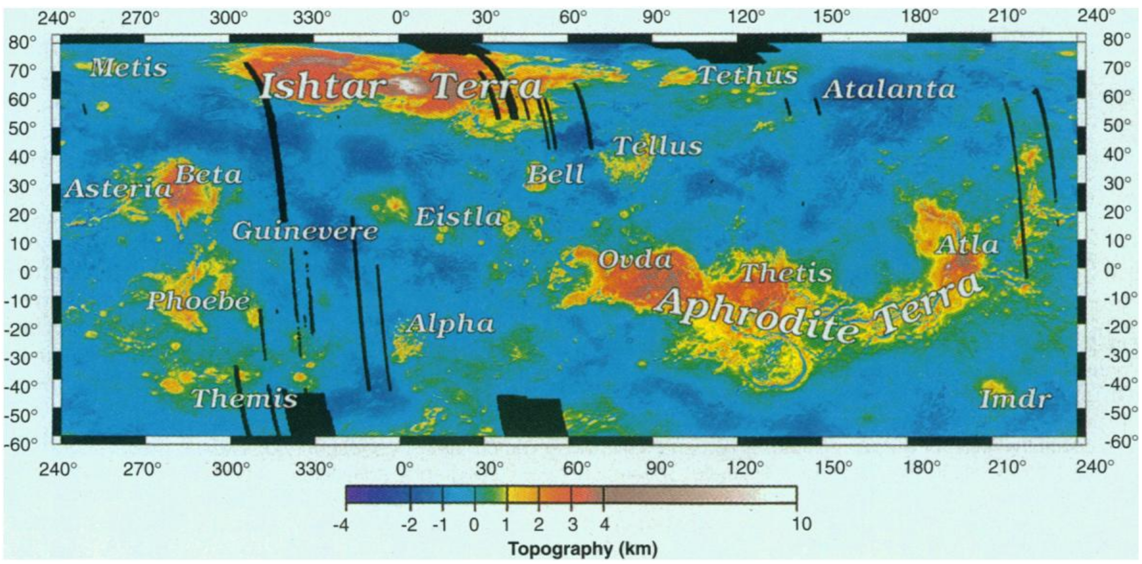

Fig. 1. Topography of Venus (60°S to 80°N), with major physiographic provinces labeled (cylindrical equidistant projection). Blackened areas lack Magellan altimetry measurements.

tances at the highest wave number band used here, as well as in a global degree-by-degree analysis (35), are consistent with an average crustal thickness of no more than about 25 km, although this result remains to be confirmed by higher resolution studies.

The admittance for all of Ishtar Terra is about 4 m/km at wavelengths less than 3000 km, corresponding to an ADC of about 40 km (Fig. 2D). Convective processes are not required to explain such admittance values. This ADC value differs from an earlier estimate of 180 ± 20 km (18), presumably because the admittance derived here incorporates low-elevation LOS data from the presently nearly circular orbit of Magellan. Aphrodite Terra can be divided into two regions. To the west of 135°E in Ovda and Thetis Regiones, admittances are 3 to 7 m/km (Fig. 2E), whereas to the east in Atla Regio, the admittances are much higher, 20 to 30 m/km (Fig. 2F). These values agree well with previous ADC estimates of 70 and 230 km for western and eastern Aphrodite, respectively (17). The admittance for Tellus Regio (Fig. 2G) is similar to that of Ishtar, Thetis, and Ovda Regiones, all about 4 m/km. Although Alpha Regio is similar to these areas at wavelengths less than 2500 km, the admittance increases at longer wavelengths (Fig. 2H). This difference arises because Alpha has a lateral extent of only about 1500 km, so that longer wavelengths primarily sample the surrounding plains.

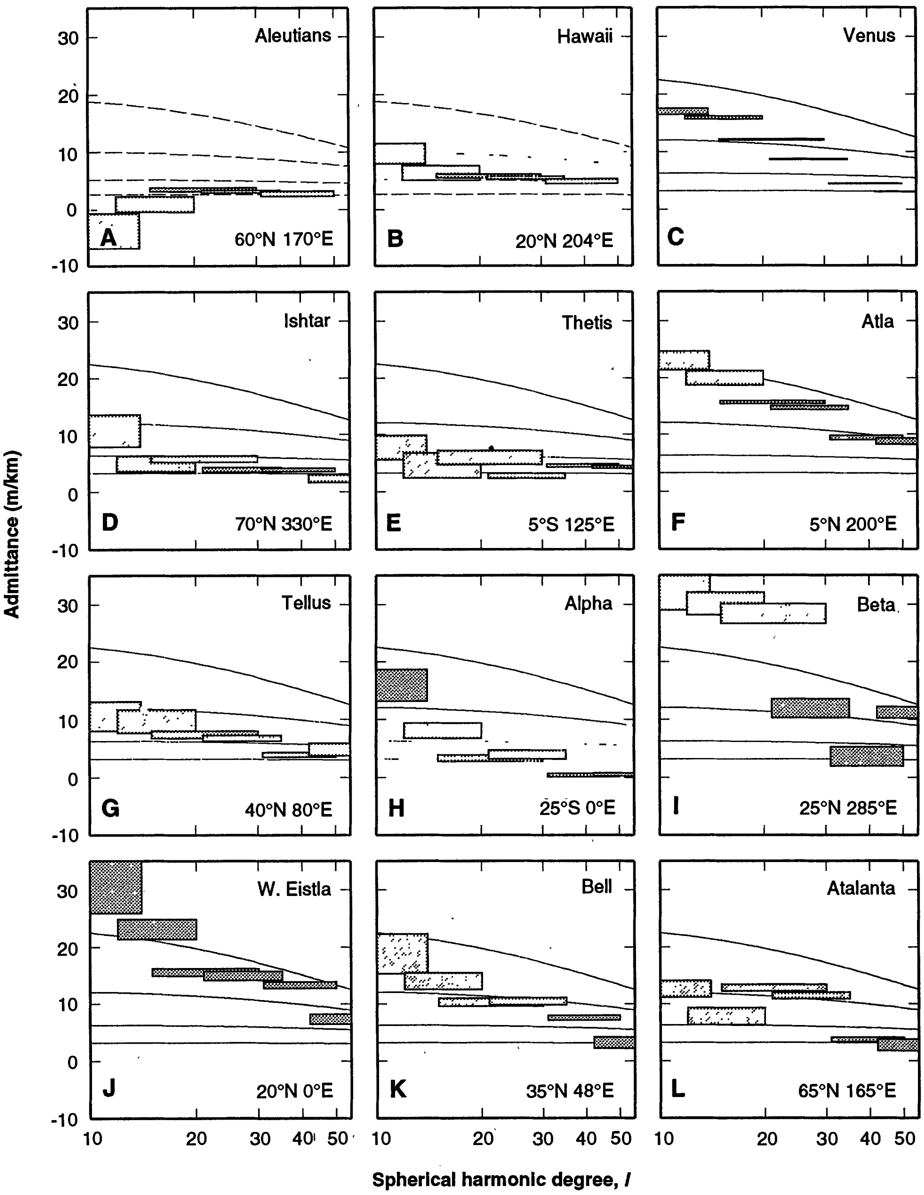

Fig. 2. Admittances for (**A**) the Aleutian trench and island arc, (**B**) the Hawaiian hot spot, (**C**) all of Venus ($D_w = 2\pi R$, where R is the radius of Venus), (**D**) Ishtar Terra, (**E**) Thetis Regio, (**F**) Atla Regio, (**G**) Tellus Regio, (**H**) Alpha Regio, (**I**) Beta Regio, (**J**) western Eistla Regio, (**K**) Bell Regio, and (**L**) Atalanta Planitia. The admittances are shown as shaded rectangles whose horizontal extent represents the limits of the harmonic degree band and whose vertical extent corresponds to two standard deviations in the admittance estimate. Theoretical geoid/topography admittance curves for Airy isostasy with different compensation depths (25, 50, 100, and 200 km in bottom-to-top order) are shown (21): Solid lines are for Venus (ρ = 2900 kg/m^3, g = 8.9 m/s^2, and R = 6051 km); dashed lines are for Earth (ρ = 2670 kg/m^3, g = 9.8 m/s^2, and R = 6371 km).

The admittance for Beta Regio, about 30 m/km at wavelengths greater than 2000 km (Fig. 2I), is in good agreement with a previous estimate of 31 ± 2 m/km obtained from PVO LOS data (19). At wavelengths less than 1000 km, the admittance increases with decreasing wavelength, perhaps a result of localized crustal thickening by magmatic activity. Extending between Beta and Atla Regiones, the rift zones of Hecate and Parga Chasmata have an admittance in band 3 of about 15 m/km (Fig. 3B), distinctly higher than the value in the surrounding plains of 10 m/km. High admittances are also found in Eistla Regio, with values in all bands greater than the planetary average (Fig. 2J). At the longest wavelengths, the results for Eistla Regio and surrounding areas agree with those of an earlier regional analysis (20). However, at shorter wavelengths, the admittances are less, and the implied ADC is shallower (Fig. 2J). Many of the previous local analyses display this long-wavelength bias (18–20). In Bell Regio, for instance, our admittance of about 20 m/km in band 1 agrees with the result of an earlier regional model (19) but decreases significantly in higher bands (Fig. 2K). This bias in previous estimates may stem from an implicit reliance on an Airy isostatic model (29), which our results suggest is not generally valid. In addition, many features on Venus may not have significant geoid and topographic expression in a particular wave number band, leading to large variations in admittance across different bands. The admittance for Atalanta Planitia (Fig. 2L) is typical of the plains and lowlands with a value of about 10 m/km at wavelengths greater than about 1500 km (Fig. 3). At shorter wavelengths, the admittance in the plains and lowlands decreases significantly to values comparable with the globally averaged values for corresponding wavelength bands (Fig. 2C).

The admittance in all bands is consistently nonnegative for the entire portion of Venus for which the geoid is well resolved and the admittance well constrained. In addition, the mean admittance values for Venus (about 16 m/km for band 1 and 13 m/km for band 3) exceed the maximum values calculated for Earth. High values of admittance from earlier global and regional analyses formed the basis for the hypothesis that Venus lacks an upper mantle low-

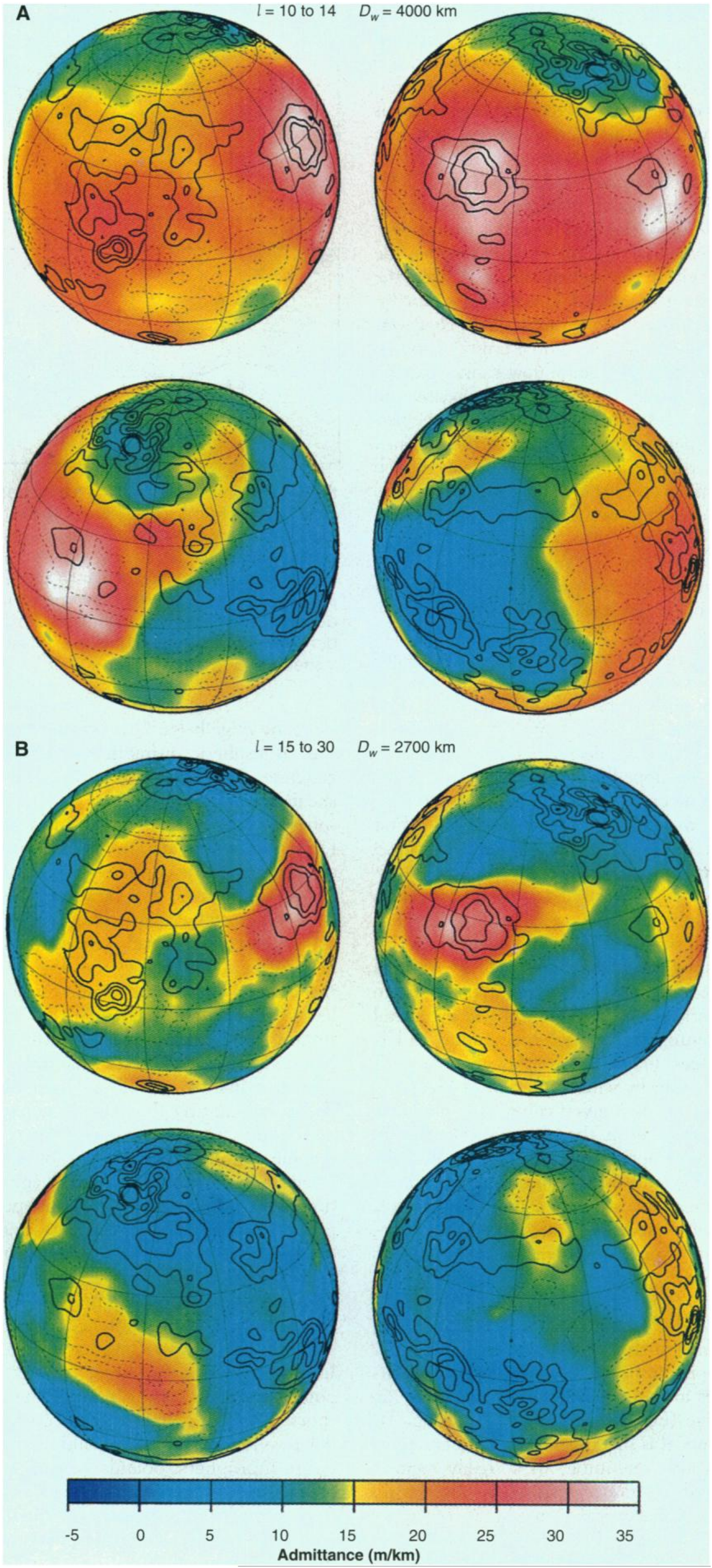

Fig. 3. Global admittance maps for Venus (orthonormal projection) over (**A**) band 1 and (**B**) band 3. Topographic contour lines at 1-km intervals are also shown for reference: dashed for elevations ≤ -0.5 km and solid for elevations ≥ 0.5 km. Lines of latitude and longitude are at 30° intervals.

viscosity zone and thus experiences strong coupling between motions of the convecting mantle and the overlying lithosphere (*1, 16, 19, 37, 39–43*). These new admittance maps are consistent with this hypothesis.

Western Aphrodite, Ishtar Terra, and the other large tesserae regions such as Alpha and Tellus are characterized by pervasive compressional features that are consistent with crustal deformation in response to horizontal shortening of the lithosphere (*2, 26, 41, 42*). The high topography in these areas probably results from a combination of crustal thickening and accumulation of low-density mantle residuum. The admittances in these areas are consistent with a crustal thickness of about 40 km. In contrast, on the basis of large admittance values and evidence for extensive volcanism, Beta, Atla, Bell, and Eistla Regiones likely overlie sites of mantle upwelling; their high topography probably results principally from a combination of vertical convective stresses on the base of the lithosphere and crustal thickening by volcanism and magmatic intrusion (*2, 5, 19, 20, 39–41, 43, 44*).

The density of impact craters on the surface of Venus indicates an average age of about 500 million years (*45*). Furthermore, the low density of craters modified by volcanic flows or deformation suggests that the rate of removal or modification of impact craters has been markedly lower since 500 million years ago (Ma) than before that time (*45*). Although the premise of coupling mantle convection to the lithosphere provides a basis for our interpretation of the admittance maps, we must distinguish between models in which the styles of surface deformation have been similar for more than 500 million years and models in which a significant change occurred at about 500 Ma. We refer to these two classes of models as a steady regime and a variable regime, respectively (*46*). Under a steady regime, all observed surface deformational features can be related to present characteristics of mantle flow. In contrast, under a variable regime, some observed tectonic features are products of processes no longer occurring. In particular, we discuss a class of models in which the highland plateaus with dominantly compressive tectonic features, such as western Aphrodite Terra and Ishtar Terra, and the tesserae are remnants of a previous regime of high crustal strain prior to 500 Ma.

We divide models of mantle-lithosphere

coupling into those that include the effects of thickening and thinning of the crust and those that do not. A model in which the crust acts only as a passive tracer, such that essentially all long-wavelength topography is simply the result of the vertical tractions associated with mantle convection, can fit the observed geoid and topography (*16, 37, 40, 43*). In this model, highlands overlie sites of mantle upwelling, and lowlands overlie sites of mantle downwelling. In such a model, the ridge belts in the lowlands are most likely the expression of limited lithospheric strain induced by mantle downwelling (*27*). However, a model without substantial crustal deformation induced by mantle flow cannot explain the large-scale compressional features seen in radar images of many highlands and the pervasive deformation recorded in the tesserae. Thus, this model can only be viable if such regions are postulated to have formed during a now extinct phase of tectonic deformation (Fig. 4A).

In contrast, if Venus is in a steady regime and the compressional highlands are relatable to present mantle flow patterns—that is, if the crust currently experiences significant deformation in response to mantle-convective tractions—then the issue of the origin of the lowlands remains (Fig. 4B). The lowlands have previously been hypothesized to be regions of incipient or fully developed downgoing mantle flow, which eventually mature to states resembling western Aphrodite Terra or Ishtar Terra (*5, 27, 41*). To accomplish such a metamorphosis, the topography must change sign (relative to the global mean elevation) during the evolution of the convective downwelling. The sign of the topography would be dominated by vertical convective stresses (surface depression) in the early stages of evolution and by crustal thickening effects (high topography) in later stages (*41, 47*). In the absence of a mechanism by which the sign of the geoid anomaly from a given convective phenomenon changes at the same time as that of the topography, this scenario involves an early lowland period during which admittance is of one sign (for example, negative), a brief period with no appreciable topographic expression when the admittance is unbounded (or the geoid and topography signatures are incoherent), and a late highland period when the admittance has a sign opposite to that of the lowland period (for example, positive). Because observed admittances for both lowlands and highlands are positive (Fig. 2, C through L, and Fig. 3), this model is inconsistent with observation.

By this reasoning, in a steady regime, lowlands overlie regions where there is no substantial vertical component of upper mantle flow, and a source of stress other than localized downwelling is required to

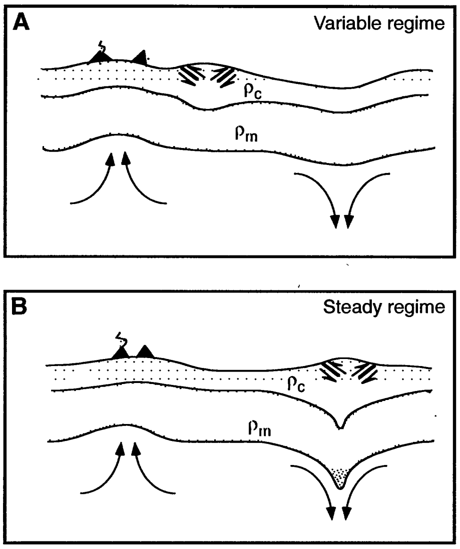

Fig. 4. Schematic illustration of the two permissible regimes that are consistent with the geoid/topography admittance constraints: (**A**) variable regime and (**B**) steady regime. Curving arrows indicate direction of mantle flow, ρ_c and ρ_m indicate regions with crustal and mantle densities, respectively, and thrust fault symbols denote compressional highland plateaus and tesserae.

form the ridge belts. One possibility is that the lithospheric instabilities believed to generate the ridge belts (*27*) arise from shear tractions at the base of the lithosphere. However, this mechanism has yet to be explored in detail. In addition, in a steady regime, the consistently positive values of admittance, together with observations of crustal deformation, require that surface elevation over downwellings always be positive. This implies that the thickening of crust and any buoyant residuum is always sufficient to overcome the effect of surface downwarping by flow in the underlying mantle. On the other hand, topography over mantle upwellings must also be positive, requiring that mantle convective uplift and magmatic additions to crustal volume dominate the effects of convectively induced crustal extension and thinning. One possible solution to this apparent paradox is that over mantle upwellings the crust is shielded from convective shear tractions by the strong mantle portion of the lithosphere, such that crustal thinning is either negligible or outweighed by constructional volcanism and magmatic intrusion. In contrast to upwellings, where rising plumes impinge on the base of the lithosphere, the development of convective downwelling instabilities would involve the entire lithospheric boundary layer. In this scenario, the crust would not be shielded from convective tractions but would deform with the rest of the lithosphere as the instability grows.

Both the steady and the variable regimes require that there be no significant extensional thinning of the crust over regions of upwelling mantle. Several tectonic observations suggest that such a requirement is met. Impact craters in regions of postulated mantle upwelling show only limited amounts of strain (*48*). Strain in these regions occurs primarily across rifts, which show only limited amounts of horizontal separation (*2, 23*). In addition, except for isolated volcanic edifices, rifts show little evidence for voluminous magmatism, in support of the view that the crust and lithosphere have not thinned sufficiently to generate widespread pressure-release melting. Similarly consistent with both regimes is the evidence for only limited crustal deformation in the lowlands (*2*).

A variable regime, however, is favored by the results of several recent studies. The tesserae have a higher density of impact craters larger than 16 km in diameter than do the plains, and only one-sixth of the large impact craters in the tesserae have been significantly deformed; these results suggest that recent tectonic activity has not been widespread in these regions (*49*). Further, new laboratory measurements indicate that the strength of crustal rocks under dry, Venus-like conditions is much greater than previously recognized, implying that the large topographic relief and steep slopes found in the crustal plateaus and mountain belts can be maintained over longer time periods than previously assumed on the basis of the high surface temperature and the strength of crustal rocks on Earth (*50*). Consistent with these new measurements of creep strength are Earth-like estimates of the thickness of the elastic lithosphere on Venus from the flexural response to volcanic and tectonic loading (*51*).

While the conclusion that mantle convection and lithospheric deformation are strongly coupled on Venus remains firm (*1, 16–20, 37, 39–43*), the admittances are consistent with two quite different models for the evolution of surface deformation. A model in which the crust currently experiences extensive deformation in response to convective coupling can be valid only in what we term a steady regime. In this regime, lowlands are not dynamic features, and the rheological stratification of the lithosphere must be such that the crust is shielded from shear tractions over mantle upwellings but is able to deform rapidly during the development of cold downgoing mantle instabilities. In contrast, a model in which the crust does not thicken or thin significantly in response to present convective tractions can be valid only in what we term a variable regime. In such a regime, which we currently favor, the compressional highlands and tesserae are products of past, rather than current, mantle processes, and most other long-wavelength topographic features are principally the result of vertical tractions at the base of the lithosphere.

REFERENCES AND NOTES

1. R. J. Phillips and M. C. Malin, in *Venus*, D. M. Hunten, L. Colin, V. I. Moroz, T. M. Donahue, Eds. (Univ. of Arizona Press, Tucson, AZ, 1983), p. 159.
2. S. C. Solomon *et al.*, *Science* **252**, 297 (1991); S. C. Solomon *et al.*, *J. Geophys. Res.* **97**, 13199 (1992).
3. Aspects of plate tectonics that should be recognizable from imaging and altimetric data include a globally interconnected network of centers of crustal spreading, large-offset strike-slip faults, and zones of crustal convergence. Spreading centers should display a predictable decrease in topographic height with distance [W. M. Kaula and R. J. Phillips, *Geophys. Res. Lett.* **8**, 1187 (1981); R. E. Grimm and S. C. Solomon, *J. Geophys. Res.* **94**, 12103 (1989); (*2*)].
4. W. M. Kaula, *Science* **247**, 1191 (1990).
5. R. J. Phillips, R. E. Grimm, M. C. Malin, *ibid.* **252**, 651 (1991).
6. C. H. Scholz, *The Mechanics of Earthquakes and Faulting* (Cambridge Univ. Press, Cambridge, 1992); N. H. Sleep and M. L. Blanpied, *Nature* **359**, 687 (1992).
7. D. P. McKenzie, in *Island Arcs, Deep Sea Trenches, and Back Arc Basins*, M. Talwani and W. C. Pitman III, Eds. (American Geophysical Union, Washington, DC, 1977), p. 57.
8. The topography of Venus has been measured by combining spacecraft tracking data with measurements of the time for a radar burst to travel from the spacecraft to the planet surface and back [P. G. Ford and G. H. Pettengill, *J. Geophys. Res.* **97**, 13103 (1992)]. The gravity field of Venus is being measured by tracking of the spacecraft. Variations in the gravity field cause changes in the spacecraft velocity that can be measured on Earth as a Doppler shift in the transmitted signal. This type of observation is referred to as a line-of-sight velocity, because it is sensitive only to the component of velocity along a line connecting the spacecraft and the Earth. The LOS data are subsequently inverted to obtain a model of the planet's gravity field [see, for example, R. J. Phillips, W. L. Sjogren, E. A. Abbott, S. H. Zisk, *J. Geophys. Res.* **83**, 5455 (1978)].
9. The geoid is the equipotential surface of the gravitational field at zero elevation. A positive mass anomaly produces a positive geoid anomaly. Geoid height on Venus is referenced to a spherical surface.
10. The lithosphere is the mechanically strong portion of the cold upper thermal boundary layer of the convecting mantle and includes the crust and the uppermost portion of the mantle.
11. D. P. McKenzie, *Geophys. J. R. Astron. Soc.* **48**, 211 (1977).
12. M. McNutt, *J. Geophys. Res.* **85**, 6377 (1980).
13. ——— and L. Shure, *ibid.* **91**, 13915 (1986).
14. E. M. Robinson and B. Parsons, *ibid.* **93**, 3144 (1988); W. S. Kiefer, *Geophys. Res. Lett.* **20**, 265 (1993).
15. W. L. Sjogren *et al.*, *J. Geophys. Res.* **88**, 1119 (1983).
16. W. S. Kiefer, M. A. Richards, B. H. Hager, B. G. Bills, *Geophys. Res. Lett.* **13**, 14 (1986).
17. R. R. Herrick, B. G. Bills, S. A. Hall, *ibid.* **16**, 543 (1989).
18. R. E. Grimm and R. J. Phillips, *J. Geophys. Res.* **96**, 8305 (1991).
19. S. E. Smrekar and R. J. Phillips, *Earth Planet. Sci. Lett.* **107**, 582 (1991).
20. R. E. Grimm and R. J. Phillips, *J. Geophys. Res.* **97**, 16035 (1992).
21. R. S. Saunders *et al.*, *ibid.* **95**, 8339 (1990); R. S. Saunders and G. H. Pettengill, *Science* **252**, 247 (1991).
22. Before August 1993, Magellan was in an elliptical orbit. Since then, the spacecraft has been in a nearly circular orbit. The gravity field inferred from tracking of the spacecraft is well resolved north of 60°S. Coverage in the near-circular orbit is incomplete as of this writing.
23. D. A. Senske, G. G. Schaber, E. R. Stofan, *J. Geophys. Res.* **97**, 13395 (1992).
24. D. L. Bindschadler, A. deCharon, K. K. Beratan, S. E. Smrekar, J. W. Head, *ibid.*, p. 13563.
25. A. A. Pronin, *Geotectonics* **20**, 271 (1986).
26. W. M. Kaula *et al.*, *J. Geophys. Res.* **97**, 16085 (1992).
27. M. T. Zuber, *ibid.* **92**, E541 (1987); *Geophys. Res. Lett.* **17**, 1369 (1990); S. W. Squyres *et al.*, *J. Geophys. Res.* **97**, 13579 (1992).
28. J. R. Ockendon and D. L. Turcotte, *Geophys. J. R. Astron. Soc.* **48**, 479 (1977); D. T. Sandwell and M. L. Renkin, *J. Geophys. Res.* **93**, 2775 (1988); D. T. Sandwell and K. R. MacKenzie, *ibid.* **94**, 7403 (1989).
29. The simplest model of topographic compensation is Airy isostasy, whereby a topographic load is locally balanced by an equal and opposite load at a single depth, termed the apparent depth of compensation (ADC). For Airy isostasy, assuming Cartesian geometry (appropriate at short wavelengths), the admittance Z is

$$Z(k) = \frac{N(k)}{H(k)} = \frac{2\pi G\rho}{gk}(1 - e^{-kD}) \quad (9)$$

where N and H are the harmonic geoid and topography, G is the gravitational constant, ρ is the density of surface material, g is the gravitational acceleration, k is the wave number, $\lambda = 2\pi/k$ is the wavelength, D is the ADC, and $\lambda >> H$ (*28*). In this study, we used the spherical analog to Eq. 9

$$F_l = h_l\frac{4\pi G\rho R}{g}\left(\frac{1}{2l+1}\right)\left[1 - \left(1 - \frac{D}{R}\right)^l\right] \quad (10)$$

where F_l is the admittance function for spherical harmonic degree l, R is the radius, and h_l is the isostatic Love number [R. J. Phillips and K. Lambeck, *Rev. Geophys. Space Phys.* **18**, 27 (1980); B. H. Hager, *Earth Planet. Sci. Lett.* **63**, 97 (1983)], which is well approximated by

$$h_l \approx \frac{l + 0.6}{l} \quad (11)$$

The dependence of F_l on l is illustrated in Fig. 2 for several different ADCs, for parameters appropriate for Venus and Earth. At long wavelengths (small l), each curve flattens out (especially for shallow ADCs). Many workers have capitalized on this behavior to make a long-wavelength approximation by expanding Eq. 9 about D to eliminate the wave number dependence. The resulting expression is the GTR (*28*).
30. L. M. Dorman and B. T. R. Lewis, *J. Geophys. Res.* **75**, 3357 (1970); B. G. Bills, W. S. Kiefer, R. L. Jones, *ibid.* **92**, 10335 (1987).
31. For $l_{min} = l_{max}$ and Ω equal to the entire surface of the planet, Eq. 5 reduces to

$$\sigma^2_{ab} = \left(\frac{1}{2l+1}\right)\sum_{m=-l}^{l} A_{lm}B^*_{lm} \quad (12)$$

which is the more familiar form used in previous work to calculate degree-by-degree global averages of the covariance function [W. M. Kaula, *Rev. Geophys.* **5**, 83 (1967)]. In addition to the admittance, we calculated the formal error

$$\sigma^2_{F_l} = \left(\frac{\sigma^2_{gg}}{\sigma^2_{tt}}\right)\left(\frac{1 - r^2}{n - K_\Omega}\right) \quad (13)$$

where r is the correlation coefficient, defined as

$$r = \left(\frac{\sigma^2_{gt}}{\sqrt{\sigma^2_{gg}\sigma^2_{tt}}}\right) \quad (14)$$

and

$$K_\Omega = \frac{1}{4\pi}\iint_\Omega d\Omega \quad (15)$$

32. To calculate terrestrial admittances, we used the geoid coefficients to spherical harmonic degree and order 70 from geoid model JGM-2G (R. S. Nerem *et al.*, *J. Geophys. Res.*, in press) and an expansion of equivalent rock topography to spherical harmonic degree and order 360 [N. K. Pavlis and R. H. Rapp, *Geophys. J. Int.* **100**, 369 (1990)]. This form of topography replaces water or ice with a layer of rock of equal mass.
33. M. A. Richards and B. H. Hager, in *The Physics of Planets*, S. K. Runcorn, Ed. (Wiley, New York, 1988), p. 247; M. K. McNutt and A. V. Judge, *Science* **248**, 969 (1990).
34. Spherical harmonic coefficients of topography for Venus are from a solution by N. J. Rappaport (personal communication) to degree and order 360 fit to Magellan, PVO, and Venera altimetry measurements.
35. The geoid model, MGNP60Fsaap, uses both Magellan and Pioneer Venus data and extends to degree and order 60. This model uses an initial surface acceleration distribution to constrain the gravity solution over regions poorly sampled by spacecraft tracking data (A. S. Konopliv and W. L. Sjogren, in preparation).
36. The formal errors (*31*) for band 1 range from 1 to 6 m/km, and for band 3, from 1 to 3 m/km.
37. W. S. Kiefer and B. H. Hager, *J. Geophys. Res.* **96**, 20947 (1991).
38. M. Simons, B. H. Hager, S. C. Solomon, *Lunar Planet. Sci.* **25**, 1317 (1994).
39. R. J. Phillips, *J. Geophys. Res.* **95**, 1301 (1990).
40. W. S. Kiefer and B. H. Hager, *Geophys. J. Int.* **108**, 198 (1992).
41. D. L. Bindschadler and E. M. Parmentier, *J. Geophys. Res.* **95**, 21329 (1990).
42. W. S. Kiefer and B. H. Hager, *ibid.* **96**, 20967 (1991).
43. R. R. Herrick and R. J. Phillips, *Geophys. Res. Lett.* **17**, 2192 (1990).
44. D. A. Senske, J. W. Head, E. R. Stofan, D. A. Campbell, *ibid.* **18**, 1159 (1991).
45. R. J. Phillips *et al.*, *Science* **252**, 288 (1991); G. G. Schaber *et al.*, *J. Geophys. Res.* **97**, 13257 (1992); R. J. Phillips *et al.*, *ibid.*, p. 15923.
46. Proposed explanations for the observed distribution of craters and the high fraction of craters unmodified since their formation (*45*) include (i) a catastrophic event involving complete resurfacing of the planet by means of a global lithospheric instability [E. M. Parmentier and P. C. Hess, *Geophys. Res. Lett.* **19**, 2015 (1992); D. L. Turcotte, *J. Geophys. Res.* **98**, 17061 (1993)] or mantle overturn [V. Steinbach and D. A. Yuen, *Geophys. Res. Lett.* **19**, 2243 (1992)] or (ii) a geologically rapid decline in crustal deformation accompanying secular cooling of the planet because of the strong temperature- and stress-dependence of viscosity [S. C. Solomon, *Lunar Planet. Sci.* **24**, 1331 (1993)].
47. M. Simons, B. H. Hager, S. C. Solomon, *Lunar Planet. Sci.* **24**, 1307 (1993).
48. R. E. Grimm, *J. Geophys. Res.*, in press.
49. M. A. Ivanov and A. T. Basilevsky, *Geophys. Res. Lett.* **20**, 2579 (1993).
50. S. J. Mackwell, D. L. Kohlstedt, D. S. Scherber, M. E. Zimmerman, *Eos* **74** (fall meet. suppl.), 378 (1993).
51. D. T. Sandwell and G. Schubert, *Science* **257**, 766 (1992); S. C. Solomon, P. J. McGovern, M. Simons, J. W. Head, *Eos* **74** (fall meet. suppl.), 374 (1993).

52. We thank D. T. Sandwell for discussions that led to the original idea for the admittance maps, A. S. Konopliv and W. L. Sjogren for making available the most recent Venus geoid solutions, N. J. Rappaport for her solution for harmonic topography, and R. J. O'Connell, G. Masters, and S. Evans for helpful computer code. Figures 1–3 in this paper were generated with the Generic Mapping Tools system [P. Wessel and W. H. F. Smith, *Eos* **72**, 441 (1991)]. This work was sponsored by NASA under grants NAGW-3276 and NAGW-3425 and by the Magellan Project under contract JPL 957070 from the Jet Propulsion Laboratory.